Ultrasonics Sonochemistry 132 (2026) 107975

Contents lists available at ScienceDirect

Ultrasonics Sonochemistry

journal homepage: www.elsevier.com/locate/ultson

Ultrasound-assisted electrochemical hydrogen production in a 300 kHz sonoreactor in the presence of methanol☆

Jongbok Choi [a,1], Chaewoon Hwang [b,1], Younggyu Son [b,*,2], Muthupandian Ashokkumar [a,*,2]

[a] School of Chemistry, Faculty of Science, University of Melbourne, VIC 3010, Australia
[b] Department of Environmental Engineering, Kumoh National Institute of Technology, Gumi 39177, the Republic of Korea

ARTICLE INFO

Keywords:
Acoustic cavitation
Electrochemical
Hydrogen generation
Methanol
Reduction

ABSTRACT

This work investigates sonoelectrochemical hydrogen production in a 300 kHz sonoreactor using water–methanol electrolytes, with a focus on disentangling purely sonochemical contributions from ultrasound–induced electrochemical enhancement. Ultrasound–only experiments show that methanol addition increases cavitation–driven hydrogen formation by more than an order of magnitude relative to pure water, with an optimum around 1.2 M, but absolute rates remain at the μmol min^{-1} level and energy efficiencies are far below those of electrolysis. In contrast, electrochemical (EC) and sonoelectrochemical (US@EC) operation at 5.0 V with 0.1 M Na_2SO_4 produce 10–20 μmol min^{-1} of hydrogen with Faradaic efficiencies of approximately 50–57%, and ultrasound consistently enhances hydrogen production by 6–32% across the entire methanol concentration range. Gas–saturation experiments reveal that Ar increases the sonochemical hydrogen yield compared with N_2, yet both gases provide similar US@EC enhancements, indicating that hydrodynamic effects (bubble detachment, suppression of gas blanketing and diffusion–layer renewal) dominate over direct sonochemical hydrogen formation. Microscopic analysis further shows that 300 kHz ultrasound causes far less mechanical damage to Ti/PbO_2 and graphite electrodes than low–frequency ultrasound reported in the literature, highlighting high–frequency operation as a promising strategy to obtain stable, practically meaningful ultrasound–induced enhancement in electrochemical hydrogen production.

1. Introduction

The transition to a low–carbon energy system has intensified interest in sustainable hydrogen production technologies, with water electrolysis emerging as a key route to green hydrogen when powered by renewable electricity [1,2]. However, conventional electrolysis suffers from significant kinetic and transport limitations, particularly at high current densities where gas–bubble accumulation, ohmic losses, and sluggish mass transfer lead to increased overpotentials and reduced efficiency [3,4]. Various strategies have been proposed to mitigate these limitations, including advanced electrocatalysts, tailored electrode architectures and optimized electrolyte formulations [4,5], yet gas evolution and bubble coverage at the electrode surface remain major bottlenecks for high–rate hydrogen production.

Ultrasound has been recognized as a promising tool to improve electrochemical processes, as cavitation–induced microjets, shock waves and acoustic streaming can enhance bubble detachment, thin the hydrodynamic diffusion layer and periodically clean the electrode surface [6,7]. In water electrolysis, ultrasound has been shown to increase current density and hydrogen evolution rates by roughly 5–25% and to reduce cell voltage by alleviating gas blanketing and mass–transfer limitations, particularly in alkaline and PEM systems operated at low ultrasonic frequencies (typically 20–40 kHz) where physical effects such as intense cavitation and acoustic microstreaming dominate [8,9].

At the same time, purely sonochemical hydrogen production via water ultrasonication exhibits very low absolute rates and energy efficiencies (typically on the order of 0.001–0.2%), so that in sono–electrolysis systems the main benefit of ultrasound is generally attributed to the enhancement of electrochemical hydrogen evolution rather than direct sonolysis [8,9]. Comparable orders of magnitude and

☆ This article is part of a special issue entitled: 'Sonoelectrochemical Processes' published in Ultrasonics Sonochemistry.

* Corresponding authors.
E-mail addresses: yson@kumoh.ac.kr (Y. Son), masho@unimelb.edu.au (M. Ashokkumar).

[1] These authors contributed equally as first-authors.
[2] These authors contributed equally as corresponding authors.

https://doi.org/10.1016/j.ultsonch.2026.107975
Received 8 May 2026; Received in revised form 14 July 2026; Accepted 21 July 2026
Available online 22 July 2026
1350-4177/© 2026 The Authors. Published by Elsevier B.V. This is an open access article under the CC BY-NC-ND license (http://creativecommons.org/licenses/by-nc-nd/4.0/).

very low energy efficiencies for purely sonochemical hydrogen generation have been reported in systematic sono–electrolysis and sonochemistry studies, reinforcing that cavitation–driven H_2 production alone is not a viable primary route under typical laboratory conditions [7,10]. Although many studies have focused on low–frequency (20 kHz) power ultrasound where strong mechanical forces can even erode electrodes and membranes, systematic investigations at higher frequencies in the hundreds of kilohertz (e.g., 408 kHz) remain scarce despite recent reports that such high–frequency fields can efficiently assist gas–bubble removal and improve HER kinetics with negligible mechanical damage to porous Raney–Ni electrodes [7].

Methanol is often introduced into electrochemical systems as an easily oxidizable organic co–fuel, with the potential to replace the sluggish oxygen evolution reaction and lower the overall cell voltage required for hydrogen generation [11–13]. In practice, however, the impact of methanol on electrolyte properties, bubble dynamics and mass transfer can be complex [14,15]. Furthermore, water–methanol mixtures under ultrasonic irradiation exhibit non–monotonic sonochemical hydrogen production, with an optimum alcohol content and strong dependence on the dissolved gas and ionic strength [16,17]. Despite growing interest in ultrasound–assisted electrolysis, there is still limited understanding of how methanol concentration, supporting electrolyte and saturation gas jointly affect the balance between sonochemical hydrogen generation and electrochemical enhancement in sono–electrolysis.

In this work, we systematically investigated hydrogen production in three configurations: ultrasound–only (US), electrochemical (EC) and ultrasound–assisted electrochemical (US@EC) systems using water-methanol mixtures with and without 0.1 M Na_2SO_4 at 300 kHz and 25 °C. We quantified sonochemical hydrogen generation rates as a function of methanol concentration, established a sonochemical baseline for comparison with EC and US@EC, and evaluated hydrogen production, and Faradaic efficiency at 5.0 V for different methanol concentrations. Moreover, we examined the effect of changing the saturation gas from Ar to N_2 on sonochemical and sonoelectrochemical hydrogen production, and compared the performance and electrode stability at 300 kHz with those obtained under low–frequency (28 kHz) ultrasound.

2. Experimental methods

2.1. Chemicals and reagents

Methanol (CH_3OH) and sodium sulfate (Na_2SO_4) were obtained from Samchun Pure Chemical Co. Ltd. (KOR) and used as received. All chemicals were of analytical reagent grade. The anode was a titanium substrate coated with lead oxide (Ti/PbO_2, 5 × 5 × 0.30 cm, apparent geometric area 25 cm^2), and a graphite cathode with the same apparent geometric area was used. Both anode and cathode were purchased from Hu-nan New Frontier Science & Technology Ltd. (CHN).

2.2. US@EC reactor and gas supply

A circular glass vessel equipped with a double-wall cooling jacket and a sealing cover was used as the ultrasound–electrochemical (US@EC) reactor, as shown in Fig. 1. A 300 kHz transducer module (Mirae Ultrasonic Tech., KOR) and a 28 kHz transducer module from the same manufacturer were alternately mounted at the bottom of the same glass reactor for the high– and low–frequency experiments, respectively. The inner diameter and height of the sonoreactor were 105 and 100 mm, respectively. The liquid height was determined using equation:

$$\lambda = \frac{c}{f}$$

where λ is the wavelength, c is the speed of sound in water (1500 m/s), and f is the applied frequency (300 kHz). The liquid height and volume were 5.0 λ at 300 kHz (25 mm) and 220 mL, respectively, and headspace volume of the reactor was 866 mL. The double wall of the reactor was connected to a recirculating water chiller, and the bulk liquid temperature was maintained at 25 ± 2 °C. The electrical input power supplied to the 300 kHz transducer was fixed at 80 ± 2 W for all experiments. The acoustic power delivered to the liquid was determined calorimetrically from the initial temperature rise of the 220 mL liquid volume under adiabatic conditions, while only the ultrasonic transducer was operated. The calorimetric power was calculated from $P_{cal}=(dT/dt)\bullet C_{p,mix}\bullet M$. dT/dt is the initial slope of the bulk temperature–time curve, $C_{p,mix}$ is the

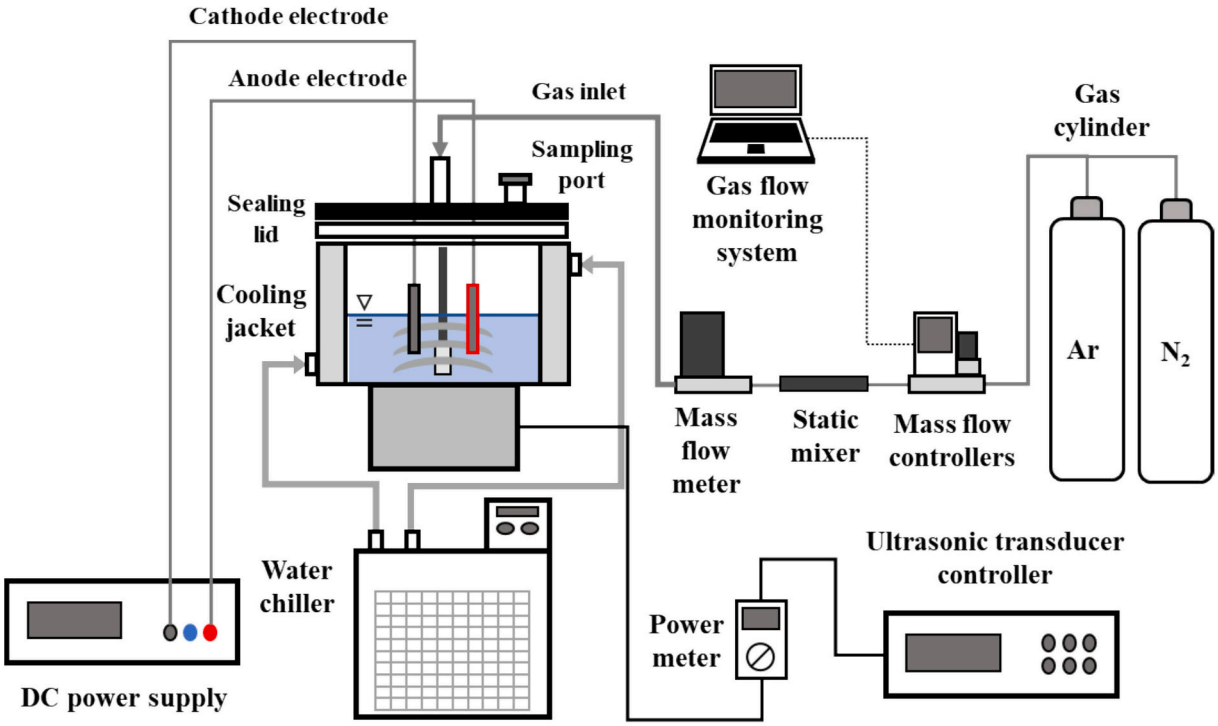


Fig. 1. Schematic of the ultrasound–electrochemical reactor with gas supply system.

mass–averaged specific heat capacity of the water-methanol mixture, and M is the total liquid mass. At 300 kHz, the calorimetric power was 29.7 ± 1.0, 27.7 ± 3.5, 27.0 ± 1.9, 26.6 ± 2.2, and 26.2 ± 0.9 W for methanol contents of 0, 0.5, 1, 5, and 10% (v/v), respectively. At 28 kHz, the calorimetric power was 35.3 ± 1.1 W (0% methanol) and 33.1 ± 1.9 W (5% methanol).

Ti/PbO_2 anodes and graphite cathodes were inserted through the sealing lid, which allowed adjustment of the electrode position and interelectrode gap. Both electrodes were selected based on previous study reporting that this commercial electrode pair exhibits favorable chemical effects when combined with ultrasound [18]. The distance between anode and cathode was fixed at 1.5 cm, and both electrodes were immersed to a depth of 1 cm. Electrodes were connected to a regulated DC power supply (EP–3010; PNCYS Co., Ltd., KOR), and the applied cell voltage was set to 5.0 V. The electrochemical performance of the electrodes was evaluated using an electrochemical workstation (IVIUMnSTAT; Ivium Technologies B.V., NLD) in a two–electrode configuration, in which the Ti/PbO_2 plate served as the anode and the graphite plate as the cathode. Linear sweep voltammetry (LSV) was conducted in 0.1 M Na_2SO_4 electrolyte over a potential window of 1–5 V at various methanol concentrations. The potential step (E_{step}) was 10 mV, the scan rate was 150 mV s^{-1}, and the current range was set to 10 mA. The electrode surface images before and after ultrasonic irradiation were observed using a digital microscope (KH-8700; Hirox, JPN).

Saturation gas was supplied to the liquid phase using a gas handling system consisting of argon (Ar) and nitrogen (N_2) cylinders, mass flow controllers (HFC–D–302B; Teledyne Hastings Instruments, USA), a static mixer (Gasline, Seongnam, KOR), a mass flow meter (HFM–D–300B; Teledyne Hastings Instruments, USA), a gas flow monitoring controller, and a microporous glass sparger (pore size 20–30 μm) attached to a glass tube. The sparger was located 1 cm above the reactor bottom. The gas flow rate during saturation was 3 L min^{-1}. After gas saturation was achieved, the sparger was removed from the reactor.

The sonoelectrochemical production of H_2 was investigated in water and water/methanol mixtures containing methanol at 0.5, 1.0, 5.0, and 10.0% (v/v). The ultrasound irradiation time was fixed at 60 min to ensure that the H_2 concentration remained above the detection limit and to provide reliable quantification under the lowest H_2–production conditions.

2.3. Quantification of H_2 production

Gas samples were collected from the reactor headspace using a 500 μL gas–tight syringe (Trajan Scientific and Medical, AUS). The H_2 concentration in the gas phase was determined using a gas chromatograph (8890 GC system; Agilent, USA) equipped with a thermal conductivity detector (TCD). The amount of sonochemically generated H_2 was calculated from the measured H_2 concentration and the headspace volume.

For all conditions, the accumulation of H_2 over the 60 min irradiation period was well described by a linear function of time, and linear fits of concentration versus time yielded coefficients of determination $R^2 \geq 0.98$, supporting the use of constant production rates (μmol min^{-1}) in the subsequent analysis. All experiments were conducted in triplicate, and error bars represent the standard deviation of three independent measurements. No additional statistical significance tests were performed, and the discussion is based on mean values with their corresponding standard deviations.

The synergistic index was calculated from the H_2 generation rates in the US, EC, and US@EC systems, as following equation:

$$SynergisticIndex = \frac{k_{US@EC}}{k_{US} + k_{EC}}$$

where k denotes the H_2 generation rate, and the subscripts refer to the corresponding H_2 production systems.

The Faradaic efficiency (FE) for H_2 generation in electrochemical and US@EC experiments was calculated using following equation [19]:

$$FE(\%) = \left(\frac{n \times F \times N}{Q_{totalchargepassed}}\right) \times 100$$

where n is the number of electrons transferred per molecule of product, F is Faraday's constant (96,485C mol^{-1}), N is the amount of product (mol), and Q is the total charge passed.

3. Results and discussion

Fig. 2. shows the hydrogen generation rates obtained under ultrasound-only operation at 300 kHz and 25 °C for 60 min as a function of methanol concentration, in the absence and presence of 0.1 M Na_2SO_4. The hydrogen production rates of 0.25, 1.38, 1.71, 2.99, and 2.64 μmol min^{-1} at 0, 0.12, 0.25, 1.23, and 2.47 M methanol, respectively, in the electrolyte–free system. When 0.1 M Na_2SO_4 was added, the rates were 0.12, 1.38, 1.44, 2.42, and 2.21 μmol min^{-1} at the same methanol concentrations. Overall, methanol addition increases the sonochemical hydrogen formation by more than an order of magnitude compared with pure water, and a clear maximum appears at an intermediate methanol concentration (around 1–1.3 M), followed by a decrease at higher methanol contents.

This non–monotonic dependence on methanol concentration is fully consistent with previous studies on hydrogen production from water and water–alcohol mixtures under ultrasonic irradiation [16,17,20]. Merouani and co–workers [17] reported that low to moderate alcohol contents (typically 5–10 vol%) enhance sonochemical hydrogen yields, whereas further increases in alcohol concentration reduce the hydrogen production rate. Similar trends have been observed for methanol and ethanol mixtures at frequencies between 20 kHz and 1 MHz, where an optimum alcohol content maximizes the number and intensity of transient cavitation events [16,20]. The rates measured in this work (on the order of 1–3 μmol min^{-1} in a small–volume reactor) are of the same order of magnitude as those reported in these sonochemical hydrogen production studies when normalized by reactor volume, confirming that the present acoustic conditions fall within the typical regime of cavitation–driven hydrogen generation.

The enhancement caused by methanol can be rationalized by considering its effect on cavitation bubble dynamics and the associated high–temperature, high–pressure chemistry inside collapsing bubbles [16]. Under ultrasonic irradiation, dissolved gases and volatile solutes accumulate in oscillating cavities, which subsequently undergo rapid collapse and generate localized hot spots with temperatures of several thousand kelvin and pressures of several hundred bar. In water–methanol systems, methanol partitions into the bubble interior and is thermally decomposed and oxidized through radical pathways, producing H•, •CH_2OH, •CH_3 and related intermediates, which can

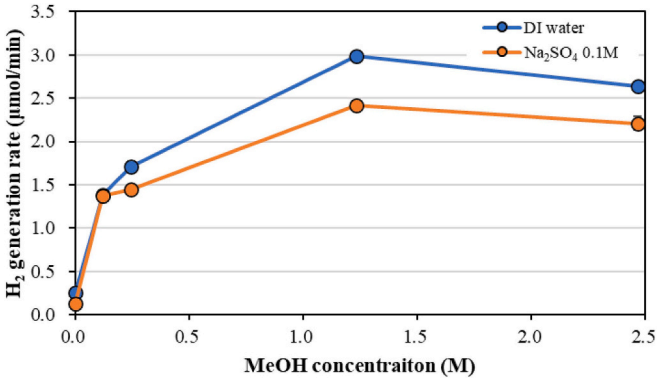


Fig. 2. Sonochemical hydrogen production rate as a function of methanol concentration with and without 0.1 M Na_2SO_4 (300 kHz, 25 °C, Ar saturated).

recombine to form molecular hydrogen [16,21]. At low methanol concentrations, this additional fuel within the bubbles increases the amount of chemically active species and thereby enhances the hydrogen yield relative to pure water.

At higher methanol concentrations, however, several adverse effects emerge. An increase in methanol content modifies key physical properties of the liquid, such as vapor pressure, heat capacity, viscosity, and surface tension, which in turn alter the cavitation process [16,21,22]. It has been shown that elevated vapor pressure and heat capacity of water–alcohol mixtures lead to softer bubble collapses, with reduced peak temperatures and pressures [23]. In addition, changes in viscosity and surface tension affect bubble nucleation, growth, and detachment behavior, and can reduce the number of transient cavitation events per unit volume [24]. As a result, beyond an optimal methanol concentration the intensity and frequency of effective cavitation collapses decrease, and the hydrogen production rate drops, as observed here at 2.47 M methanol. Thus, methanol enhances sonochemical hydrogen formation at low–to–intermediate concentrations by supplying additional volatile fuel to cavitation bubbles and increasing high–temperature bubble chemistry inside the collapsing bubbles, whereas at higher concentrations the associated changes in vapor composition and liquid properties (vapor pressure, heat capacity, viscosity, and surface tension) soften bubble collapse, reduce the number of effective cavitation events, and thereby suppress hydrogen production. This leads to the non–monotonic trend observed in Fig. 2.

The influence of Na_2SO_4 is, however, still moderate compared with the effect of methanol. Introducing 0.1 M Na_2SO_4 slightly reduces the hydrogen generation rate at intermediate and high methanol concentrations: for 0.25, 1.23 and 2.47 M methanol, the rates decrease by approximately 0.27, 0.57 and 0.43 μmol min^{-1}, corresponding to relative decreases of about 15–20%. Although non–negligible, these changes are much smaller than the one–order–of–magnitude enhancement induced by adding methanol itself and they do not alter the position of the optimum methanol concentration. This behavior agrees with previous sonochemical studies indicating that, at hundreds of kilohertz, modest variations in ionic strength mainly affect acoustic attenuation and bubble population statistics, while the dominant control over sonochemical hydrogen formation remains the vapor composition and thermodynamic properties of the water–alcohol mixture [24,25].

It is important to emphasize that, even at the optimum methanol concentration, the absolute hydrogen production rate achieved by ultrasound alone remains very low compared with electrochemical water splitting. Recent analyses of sonochemical hydrogen production have consistently reported energy efficiencies in the range of 0.001–0.2%, even under carefully optimized conditions, due to the inherently inefficient conversion of acoustic power into useful chemical reaction [17]. The rates measured here, although comparable to those in the literature, therefore represent only a tiny fraction of the hydrogen that can be produced electrochemically at similar power inputs. Consequently, in the context of the present study, the ultrasound–only data are best interpreted as providing an upper bound for the purely sonochemical contribution [22,24]. This baseline will be used in subsequent sections to evaluate to what extent the additional hydrogen obtained in the ultrasound–assisted electrochemical process (US@EC) arises from genuine electrochemical enhancement (via bubble removal and mass–transfer improvement) rather than from direct sonochemical hydrogen generation.

EC and US@EC hydrogen production rates and Faradaic efficiencies as a function of methanol concentration with 0.1 M Na_2SO_4 are summarized in Fig. 3. In the presence of the supporting electrolyte, both EC and US@EC exhibit hydrogen production in the range of 10–20 μmol min^{-1} with Faradaic efficiencies of approximately 50–57%, and ultrasound consistently provides 6–32% higher hydrogen generation than EC across all methanol concentrations. In contrast, under electrolyte–free conditions, the electrochemical (EC and US@EC) configurations produced negligible hydrogen compared with the Na_2SO_4–containing

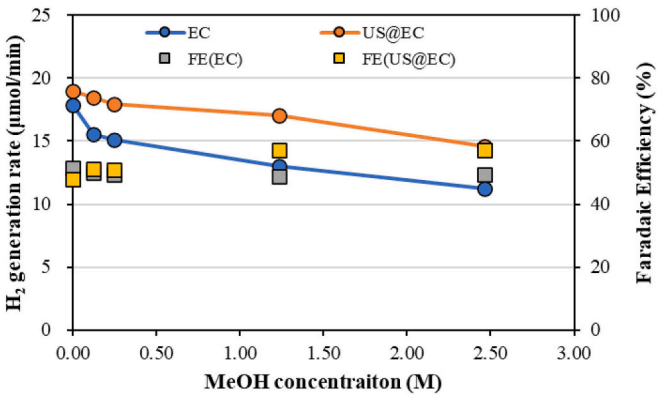


Fig. 3. Electrochemical (EC) and Sonoelectrochemical (US@EC) hydrogen production rate as a function of methanol concentration with 0.1 M Na_2SO_4 (300 kHz, 25 °C, Ar saturated).

system, and the hydrogen detected in the ultrasound–only experiments remained at the μmol min^{-1} level. This confirms that a supporting electrolyte is essential for efficient electrochemical hydrogen production and that purely sonochemical hydrogen generation is only a minor contribution under the present conditions.

In the EC system, the hydrogen generation rates at 0, 0.12, 0.25, 1.23 and 2.47 M methanol are 17.9, 15.6, 15.1, 13.0 and 11.2 μmol min^{-1}, respectively, corresponding to an overall decrease of approximately 37% across this concentration range. The corresponding average currents decrease from 0.112 to 0.073 A (about 35%), indicating that the decline in hydrogen production is directly linked to a loss of current under the fixed cell voltage of 5.0 V. This trend suggests that increasing methanol concentration progressively deteriorates the transport and/or charge transfer conditions in the EC system rather than acting as an effective co–fuel. Despite the decrease in current and hydrogen production, the Faradaic efficiencies in EC remain relatively constant, with values of 51.5, 50.1, 49.3, 48.9 and 49.5% for 0–2.47 M methanol. This indicates that approximately half of the charge passed through the cell is utilized for hydrogen evolution across all methanol concentrations, and that methanol does not introduce substantial parasitic reactions that would strongly lower the charge utilization efficiency [9,14]. Similar FE values (40–70%) have been reported in other water electrolysis systems at high current densities, where gas crossover, side reactions, and measurement uncertainties can prevent FE from reaching 100% [14,26]. The nearly constant FE therefore implies that methanol primarily affects the magnitude of the current (and hence hydrogen rate) through changes in electrolyte properties (conductivity, viscosity, bubble behavior) rather than by altering the selectivity of the electrochemical reactions [27,28]. Similar ranges of ultrasound–induced current and hydrogen production enhancements, often accompanied by reduced overall energy efficiency due to the additional acoustic power input, have been reported in parametric sono–electrolysis studies and in detailed energy–optimization analyses of ultrasound–assisted electrolysis [9,29,30].

Possible methanol-derived gaseous by–products were examined by GC using calibrated retention times of 10.1 min (CH_4) and 12.7 min (CO_2). No detectable peaks were observed at these retention times for any of the 60 min experiments, nor after extended electrolysis for 5 h at 5% methanol, whereas substantial H_2 yields were obtained (1,059 μmol in DI water and 790 μmol at 5% methanol under US@EC). These results indicate that water splitting is the predominant hydrogen–generating pathway under the present conditions, and that CO_2/CH_4 formation from methanol remains below the detection limit of our GC method. As an upper bound, if all of the measured hydrogen were hypothetically assumed to originate from methanol, the corresponding theoretical CO_2 formation would be on the order of only a few 10^2 μmol (e.g., 2.6×10^2 μmol CO_2 for 790 μmol H_2 based on $CH_3OH \rightarrow CO_2 + 3H_2$). In practice,

methanol is present at low concentrations and water electrolysis and sonochemical water splitting are expected to be the main hydrogen–forming pathways, so the actual methanol–to–CO_2 conversion must be significantly lower than this upper limit. The absence of detectable CO_2 and CH_4 signals is therefore consistent with a mechanism in which methanol primarily acts as a sacrificial co–solvent that enhances cavitation and radical chemistry, while its direct conversion to carbon–containing gaseous products plays a minor role under the present conditions.

Although the discussion of Fig. 3. is primarily based on qualitative arguments about bubble coverage and mass–transfer limitations, Fig. 4. provides direct optical evidence of the different bubble behaviors under EC–only and US@EC conditions. As shown in Fig. 4., ultrasound promotes more homogeneous bubble dispersion, reduces bubble accumulation beneath the electrodes, and shortens the bubble residence time on the electrode surfaces, supporting the mechanistic interpretation proposed for Fig. 3.

Fig. 4. compares gas bubble evolution during electrolysis under EC–only and US@EC conditions. In the EC–only system, oxygen bubbles at the anode progressively accumulated beneath the electrode, while hydrogen bubbles at the cathode remained attached to the lower part of the electrode and gradually formed a dense bubble layer. When ultrasound was applied, the bubbles around both electrodes were more homogeneously distributed, and their residence time near the electrode surfaces was markedly reduced. Bubbles were continuously displaced before prolonged accumulation beneath the electrode, resulting in more dynamic bubble motion and less persistent bubble coverage. This behavior is consistent with the combined effects of acoustic cavitation and acoustic streaming, which enhance hydrodynamic shear near the electrode surface, promote bubble detachment, and suppress bubble accumulation [9,15,31]. Consequently, the electrochemically active surface area is better maintained and mass–transfer limitations are alleviated under US@EC operation.

The two–electrode LSV curves for EC at different methanol concentrations (Fig. 5. and Fig. S1.) are presented over the reliable cell–voltage range of 1–5 V, as chronopotentiometry showed that the open–circuit cell voltage at 0 A is 0.081 V and the region below 0.5 V is influenced by this offset. Over the whole potential range from 1.0 to 5.0 V, the current–voltage curves for 0–2.47 M methanol nearly overlap, with no pronounced shift in onset potential and only small differences in current density in the 1–4 V region [7,32]. At high voltages near 5.0 V, all curves converge to similar current values. This weak dependence of the LSV response on methanol concentration suggests that, under the relatively fast potential scan, the cell performance is dominated by ohmic and kinetic contributions, while the methanol–induced mass–-transfer and bubble–coverage limitations that govern the steady–state behavior under prolonged potentiostatic operation are not fully developed [14,32,33].

When ultrasound is applied simultaneously with electrolysis (US@EC), the hydrogen production rates at 5.0 V for 60 min increase to 19.0, 18.5, 18.0, 17.1 and 14.6 μmol min^{-1} at 0, 0.12, 0.25, 1.23 and 2.47 M methanol, respectively. Compared with the EC mode, these values represent enhancements of approximately 6, 19, 19, 32 and 30% in hydrogen generation for the corresponding methanol concentrations. The average currents likewise increase to 0.128, 0.117, 0.114, 0.096 and 0.082 A, which corresponds to current enhancements of 14, 17, 15, 12 and 12% relative to EC. These gains fall within the range of 5–25% improvements in current density and hydrogen production reported in previous studies on ultrasound–enhanced water electrolysis and sono–-electrolysis, confirming that the present US@EC system behaves comparably to other ultrasonic electrolysis cells [9,15,34].

The effect of ultrasound becomes particularly significant at high methanol concentrations, where the EC performance deteriorates most strongly. At 2.47 M methanol, EC delivers only 11.2 μmol min^{-1} of hydrogen at 0.073 A, whereas US@EC achieves 14.6 μmol min^{-1} at 0.082 A, corresponding to about 30% increase in hydrogen production. This indicates that ultrasound is able to partially compensate for methanol–induced transport limitations that develop under potentiostatic operation at 5.0 V. Similar behavior has been observed in other sono–electrolysis systems, where ultrasound mitigated gas–bubble coverage and viscosity–related mass–transfer issues, leading to higher steady–state currents at fixed cell voltages in viscous or gas–evolving electrolytes[14,33,35].

The Faradaic efficiencies under US@EC are 47.8, 51.1, 50.8, 57.1 and 57.3% at 0–2.47 M methanol. At low methanol concentration, the FE is slightly lower than in EC, but at higher methanol concentrations (1.23 and 2.47 M) the FE becomes 7–8 percentage points higher than the corresponding EC values. This behavior suggests that the additional current induced by ultrasound is largely, and at high methanol concentrations even more effectively, channeled into hydrogen evolution rather than into parasitic reactions. In other words, ultrasound not only increases the magnitude of the current but can also improve the charge

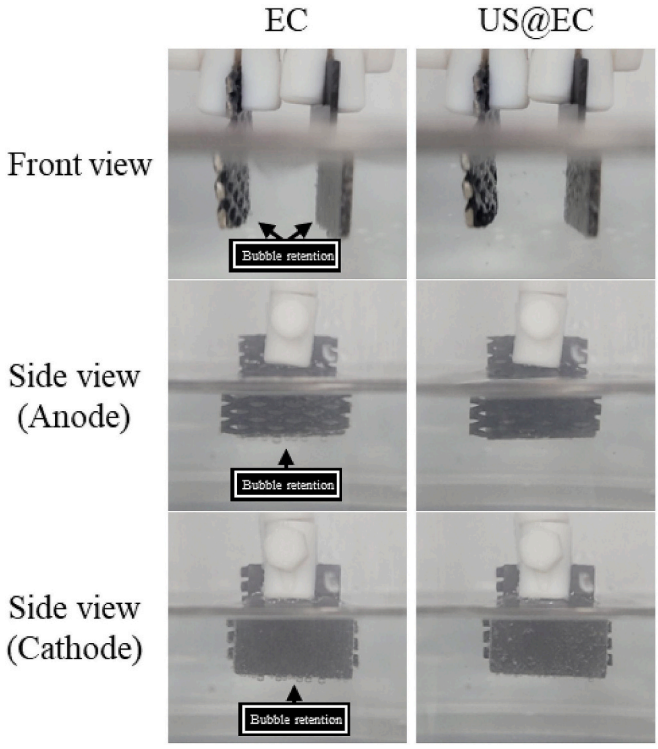


Fig. 4. Comparison of gas bubble evolution under electrochemical (EC) and ultrasound-assisted electrochemical (US@EC) conditions. (0.1 M Na_2SO_4, 300 kHz, 25 °C).

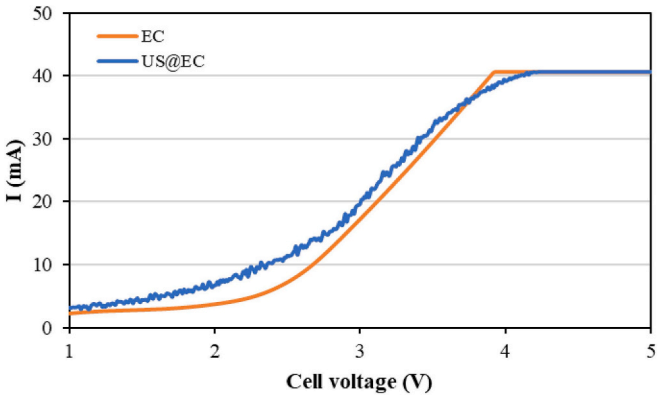


Fig. 5. Electrochemical (EC) and sonoelectrochemical (US@EC) two–electrode LSV curves in DI water (0.1 M Na_2SO_4, 300 kHz, 25 °C).

utilization towards hydrogen evolution in methanol–rich solutions, which is consistent with sonoelectrolysis studies reporting maintained or slightly improved FE in the presence of ultrasound [15,36].

As in the EC case, the two–electrode LSV curves for US@EC (Fig. 4. and Fig. S1.) exhibit only modest differences from those of EC, and the impact of ultrasound on the polarization behavior is relatively small. The US@EC curves show a slightly higher current in the intermediate potential range (2–3 V), but the overall shape and the high–voltage current near 5.0 V remain very similar to EC for all methanol concentrations. This contrast between the small LSV differences and the more pronounced enhancements observed in the 60–min potentiostatic experiments highlights that the main ultrasound effect manifests under quasi–steady–state conditions, where gas bubble accumulation, coverage and detachment dynamics can significantly influence the effective active area and mass transport [14,32,35]. LSV measurements, being transient and relatively rapid, only weakly capture these time–dependent interfacial phenomena.

The combined EC and US@EC results indicate that, at a fixed cell voltage of 5.0 V, increasing methanol concentration alone degrades electrochemical performance by reducing both current and hydrogen production, whereas the application of ultrasound yields consistent enhancements in both metrics across the whole methanol concentration range. This behavior can be interpreted in terms of ultrasound–induced modifications of the electrode/electrolyte interface. Numerous studies on water electrolysis have shown that ultrasound promotes rapid detachment of hydrogen bubbles, decreases bubble coverage and residence time on the electrode surface, and thins the hydrodynamic diffusion layer via acoustic streaming, thereby reducing bubble–induced and ohmic overpotentials [14,29,30,32,33,35]. Under prolonged potentiostatic operation at 5.0 V, these effects lead to a larger effective active area and improved mass transport, resulting in higher steady–state currents and hydrogen production rates in US@EC compared with EC. Similar behavior has been noted in ultrasonic HER studies on Pt and Raney–Ni electrodes, where ultrasound only modestly affects Tafel slopes and exchange current densities in transient voltammetry, while providing much larger performance gains under steady–state electrolysis through bubble–removal and mass–transfer effects [7,10].

In methanol–containing electrolytes, additional complications arise from changes in solution properties and bubble dynamics. Increasing methanol concentration alters viscosity, density, and surface tension, which can promote bubble coalescence, slow bubble rise velocity, and aggravate bubble coverage and mass–transfer limitations at the electrode surface [22–24,27,28,37]. The observed decrease in EC performance with methanol concentration is consistent with such methanol–induced transport and bubble effects. Ultrasound counteracts these adverse effects by continuously renewing the diffusion layer, dislodging bubbles from the surface, and disrupting bubble coalescence [14,33], which explains why the relative benefit of US@EC becomes largest at high methanol concentrations where EC suffers most strongly. The fact that Faradaic efficiency is maintained or improved under US@EC further supports the view that ultrasound primarily enhances interfacial transport and bubble dynamics rather than introducing significant additional side reactions. These observations are in line with previous sono–electrolysis work showing that ultrasound primarily improves electrochemical performance via bubble–removal and mass–transfer enhancement, while its direct sonochemical hydrogen contribution remains small and the net electrical–plus–acoustic energy efficiency often decreases relative to silent electrolysis [29,30].

Finally, when the ultrasound–only hydrogen production rates (on the order of 1–3 μmol min^{-1}) are compared with those of EC and US@EC (10–20 μmol min^{-1}), it becomes clear that the purely sonochemical contribution is small relative to the electrochemical hydrogen production under the present conditions. Therefore, the enhancements observed in US@EC at 5.0 V can be attributed predominantly to ultrasound–induced improvements in electrochemical performance (bubble removal and mass–transfer enhancement) rather than to direct sonochemical hydrogen generation.

To evaluate the influence of the saturation gas on hydrogen production, EC and US@EC experiments were performed under air, Ar and N_2 atmospheres. In the single electrochemical mode (EC), the hydrogen generation rates under air, Ar and N_2 differed by less than 4% at all methanol concentrations (0–2.47 M), indicating that the electrochemical process is essentially insensitive to the nature of the saturation gas within the experimental uncertainty. Consequently, only the air data are shown for EC in the Fig. 6. for clarity. This behavior is consistent with previous electrolysis studies, in which the choice of inert headspace gas has a negligible effect on the overall cell performance as long as mass–transfer and bubble removal are not limited by gas solubility [9,36].

In contrast, the saturation gas has a more noticeable impact on the sonoelectrochemical hydrogen production in the US@EC mode. At 5.0 V and 25 °C, the hydrogen generation rates obtained with Ar saturation are 19.0, 18.5, 18.0, 17.1 and 14.6 μmol min^{-1} at 0, 0.12, 0.25, 1.23 and 2.47 M methanol, respectively, whereas N_2 saturation yields 19.0, 17.6, 17.7, 15.6 and 13.7 μmol min^{-1} at the same methanol concentrations. Ar thus provides slightly higher hydrogen production than N_2 at most methanol concentrations, with differences of up to 9% at the highest methanol content. Nevertheless, when these values are compared to the corresponding EC rates (17.9, 15.6, 15.1, 13.0 and 11.2 μmol min^{-1}), it is clear that both Ar– and N_2–saturated US@EC systems deliver a similar level of enhancement over EC across the entire methanol concentration range.

The ultrasound–only experiments further highlight the gas effect on cavitation. With Ar saturation, the sonochemical hydrogen production rates are 0.12, 1.38, 1.44, 2.42 and 2.21 μmol min^{-1} at 0–2.47 M methanol, whereas under N_2 saturation the rates decrease to 0.02, 0.50, 0.65, 1.11 and 0.75 μmol min^{-1}. These results confirm that Ar is a more effective cavitation gas than N_2, producing 2–3 times higher sonochemical hydrogen yields at a given methanol concentration, in agreement with sonochemistry literature showing that noble gases such as Ar lead to more violent bubble collapses and higher radical and hydrogen yields than molecular gases like N_2 [38–40]. However, even with Ar the absolute sonochemical hydrogen production remains at the μmol min^{-1} level and thus is still small compared with the electrochemical hydrogen rates in EC and US@EC.

To quantify the net synergistic effect of ultrasound in the electrochemical system, the synergistic index (US@EC/EC) were calculated. Under Ar saturation, the synergistic index are 1.06, 1.09, 1.08, 1.11 and 1.09 at 0, 0.12, 0.25, 1.23 and 2.47 M methanol, respectively, while under N_2 saturation the corresponding values are 1.06, 1.09, 1.12, 1.10 and 1.14. Thus, both gases provide broadly similar levels of enhancement, with synergy factors in the narrow range of 1.06–1.14, and N_2

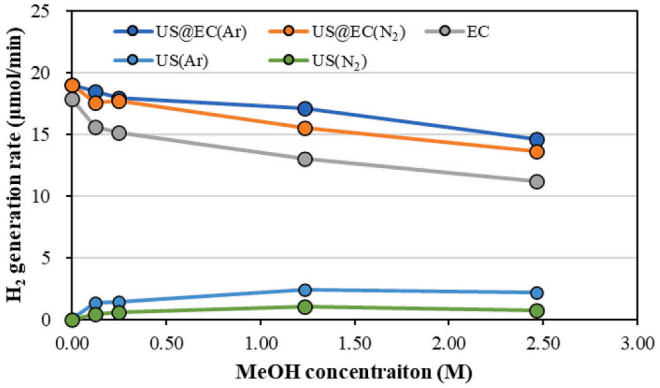


Fig. 6. Hydrogen generation rates of ultrasound–only (US), electrochemical (EC), and sonoelectrochemical (US@EC) systems as a function of methanol concentration under Ar and N_2 saturation (0.1 M Na_2SO_4, 5.0 V, 300 kHz, 25 °C).

even yields slightly higher synergistic index at some methanol concentrations despite its lower sonochemical hydrogen production in the ultrasound–only experiments. This observation indicates that the dominant contribution of ultrasound in US@EC arises from hydrodynamic and interfacial effects, such as bubble detachment, suppression of gas–blanketing and diffusion–layer renewal, rather than from the absolute magnitude of the sonochemical hydrogen generated, which is more sensitive to the choice of cavitation gas [33,36].

It should be noted that, in the present US@EC reactor, direct measurements of dissolved gas composition, bubble size distributions or in situ bubble temperatures under Ar and N_2 saturation are not feasible without strongly perturbing the acoustic field. Therefore, the roles of Ar and N_2 discussed above are inferred from the measured hydrogen production rates and synergy indices, and are supported by established literature on gas–dependent cavitation, rather than by direct observations of bubble dynamics. Overall, Ar saturation can induce somewhat stronger cavitation and slightly higher hydrogen production in US@EC, but the synergistic enhancement relative to EC remains significant and of comparable magnitude even under N_2 or air. These results imply that, for practical operation, the use of inexpensive and readily available gases such as air or nitrogen is sufficient to achieve meaningful ultrasound–induced enhancements in electrochemical hydrogen production, while Ar can be reserved for conditions where maximization of sonochemical effects is specifically desired.

Fig. 7. compares the hydrogen generation kinetics and Faradaic efficiencies of ultrasound-only (US), electrochemical (EC), and sonoelectrochemical (US@EC) processes at 28 kHz and 300 kHz under two representative methanol concentrations, 0 M and 1.23 M (5 vol% methanol). In the absence of methanol (0 M), purely sonochemical hydrogen production remained very low, with rates of 0.03 μmol min^{-1} at 28 kHz and 0.12 μmol min^{-1} at 300 kHz, whereas electrolysis alone produced 17.9 μmol min^{-1} with a Faradaic efficiency (FE) of 50.9%. When ultrasound was coupled with electrolysis, US@EC at 28 kHz yielded 12.5 μmol min^{-1} (FE 31.5%), while US@EC at 300 kHz achieved 19.0 μmol min^{-1} (FE 47.8%), indicating that high-frequency ultrasound can enhance the kinetic rate while partially preserving the charge efficiency.

At 1.23 M methanol, which offered the strongest sonochemical synergy in this system, ultrasound-only hydrogen production increased to 0.98 μmol min^{-1} at 28 kHz and 2.42 μmol min^{-1} at 300 kHz. Under the same conditions, electrolysis alone produced 13.0 μmol min^{-1} (FE 48.8%), while US@EC at 28 kHz and 300 kHz yielded 10.4 μmol min^{-1} (FE 34.6%) and 17.1 μmol min^{-1} (FE 57.1%), respectively. These data clearly show that 300 kHz sonoelectrolysis in methanol-containing electrolyte can simultaneously improve hydrogen production rate and Faradaic efficiency relative to the silent EC baseline, whereas 28 kHz operation enhanced hydrogen evolution relative to ultrasound-only conditions but resulted in lower production rate and Faradaic efficiency compared to silent electrolysis, indicating a trade-off rather than true synergy.

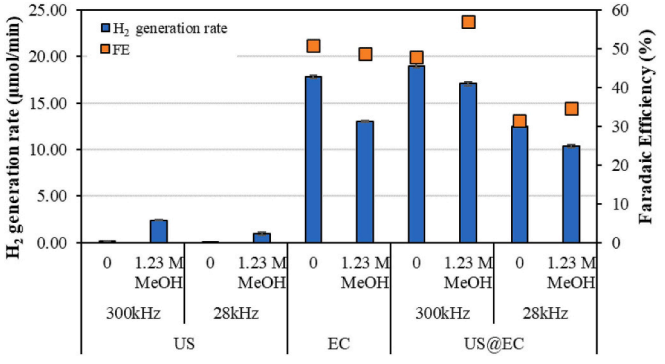


Fig. 7. Hydrogen generation rates of ultrasound–only (US), electrochemical (EC), and sonoelectrochemical (US@EC) systems at 28 kHz and at 300 kHz (0.1 M Na_2SO_4, 5.0 V, 25 °C).

The influence of ultrasound frequency on electrode integrity was further examined by microscopic analysis of the anode (Ti/PbO_2) and cathode (graphite) surfaces after exposure to 28 and 300 kHz ultrasound (Fig. 8.). At 28 kHz, the Ti/PbO_2 anode exhibited noticeable surface spalling from the outer edge region even after only 10 min of sonication, and extensive delamination was observed after 60 min, whereas virtually no morphological change was detected at 300 kHz over the same irradiation time. On the graphite cathode, 28 kHz irradiation produced distinct black dot features with characteristic diameters of approximately 91.7–234 μm within a short exposure period, and the affected area increased further after 60 min, while at 300 kHz almost no damage was visible at short times and only smaller black dots in the range of 39.8–50.6 μm appeared after 60 min. These observations indicate that low–frequency ultrasound induces more severe mechanical erosion of both electrodes than high–frequency ultrasound under otherwise identical conditions.

The contrast in damage patterns can be rationalized by the difference in cavitation bubble size and collapse intensity at these two frequencies. Theoretical and experimental studies have shown that the resonance radius of cavitation bubbles scales inversely with acoustic frequency [41,42], with typical resonance sizes of around 150 μm at 20 kHz and of the order of less than 30 μm at several hundred kilohertz, consistent with estimated resonance radii of 107 μm at 28 kHz and 10 μm at 300 kHz in the present system [42]. Larger low–frequency bubbles collapse more violently, generating strong shock waves and high–velocity microjets that can locally pit and peel electrode surfaces, particularly on mechanically weaker materials such as graphite. The size of the black dot features therefore reflects not only the initial impact of individual bubble collapses but also the subsequent concentration of ultrasonic mechanical effects around pre–existing defects, which promotes progressive growth of the damaged zones under continued irradiation. In contrast, the finer cavitation field at 300 kHz produces more moderate, spatially distributed mechanical stresses, which are sufficient to enhance bubble detachment and mass transfer but generally insufficient to cause extensive erosion of the Ti/PbO_2 anode or deep cratering of the graphite cathode over the timescales investigated.

In this context, the synergy of ultrasound in sonoelectrochemical hydrogen production can be understood as arising primarily from the removal of gas bubbles from the electrode surface, thinning of the diffusion layer and reduction of bubble–induced overpotentials, rather than from deliberate mechanical abrasion of the electrode [8,35]. However, at low frequencies below less than 100 kHz, the pronounced physical effects associated with intense cavitation such as shock waves and microjets can lead to significant electrode damage and long–term performance degradation, as also noted in previous sonoelectrochemical studies employing 20–40 kHz horn transducers [10,31]. Our microscopy results confirm that 28 kHz irradiation imposes a much stronger mechanical load on both Ti/PbO_2 and graphite electrodes than 300 kHz, which explains why low–frequency operation in this system is accompanied by lower Faradaic efficiencies and accelerated electrode deterioration, despite its ability to increase the instantaneous hydrogen evolution rate.

Table 1. summarizes recent quantitative reports on sonoelectrochemical hydrogen production. Recent sono-electrochemical studies have also attempted to quantify hydrogen production and ultrasound-induced enhancement under various operating conditions. Teoh et al. [9,15,34] investigated 40 kHz ultrasound-assisted electrolysis in 0.15 M $NaHCO_3$ using carbon electrodes, reporting that the application of ultrasound increased the hydrogen production rate from 50.6 to 74.1 μmol min^{-1} (US@EC/EC = 1.46) [9]. In subsequent work [34], they introduced ZnO, Cu_2O and graphene as suspended catalysts, and found that graphene at 1.0 g L^{-1} yielded the highest hydrogen production with rates of 38.7 μmol min^{-1} (EC) and 48.5 μmol min^{-1} (US@EC), corresponding to a more modest synergy factor of 1.25. A

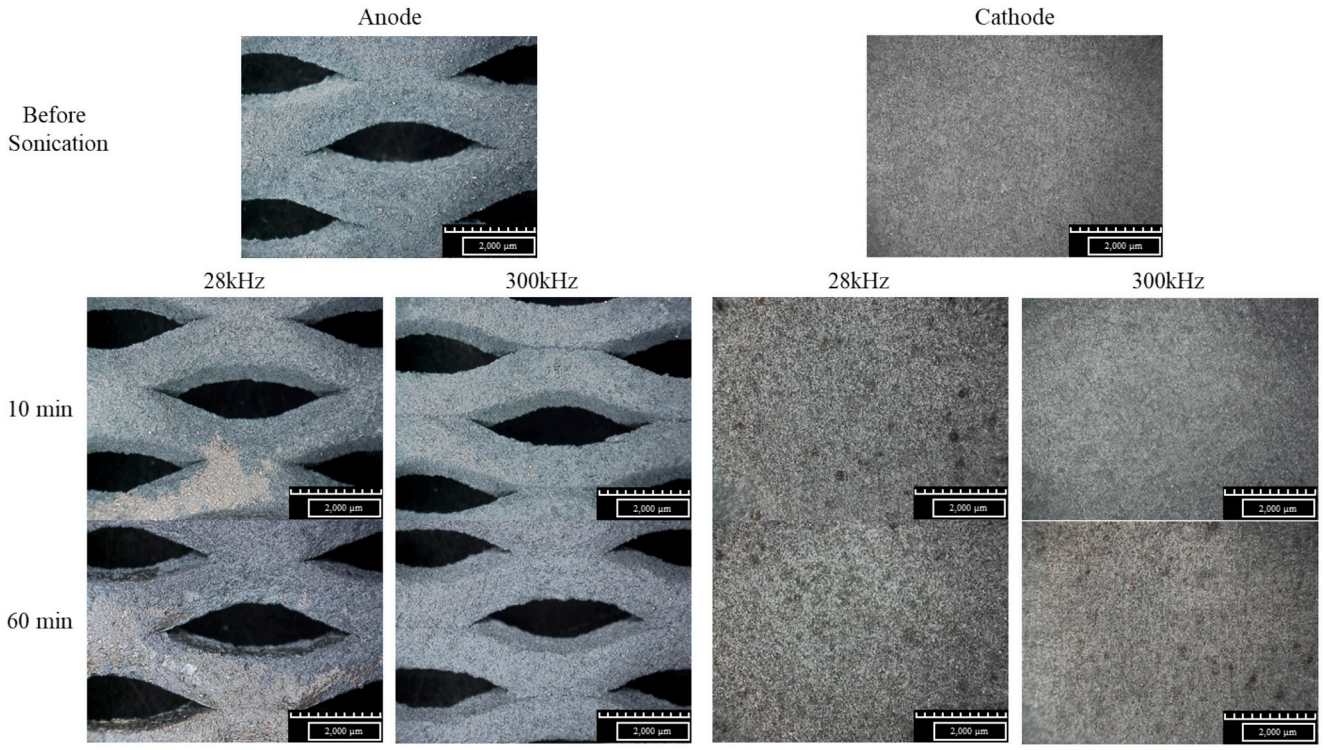


Fig. 8. Microscopic images of the anode and cathode before and after the US@EC process at 28 kHz and 300 kHz (0.1 M Na_2SO_4, 5.0 V, 25 °C).

Table 1
Recent studies on hydrogen production by US@EC processes.

Ultrasound		Electrochemical			H_2 production (μM/min (μmol/min))			Experimental condition	Ref.
Frequency (kHz)	Power (W)	Cathode	Anode	Voltage (V)	US	EC	US@EC		
40	110	Carbon	Carbon	10	–	50.6	74.1	$NaHCO_3$ 0.15 M	[9]
40	110	Carbon	Carbon	–	–	38.7	48.5	$NaHCO_3$ 0.15 M Graphene 1 g/L	[34]
40	110	Carbon	Carbon	–	–	37.8	40.7	$NaHCO_3$ 0.15 M, NiO 1 g/L	[15]
490	70	Nickel	Nickel	1.8	5.69	4.90	8.95	KOH 1 M Ar saturated	[31]
28	80	Graphite	Ti/PbO_2	5	0.03 (0.03)	20.6 (17.9)	14.4 (12.5)	Na_2SO_4 0.1 M Ar saturated	This study
28	80	Graphite	Ti/PbO_2	5	1.13 (0.98)	15.3 (13.0)	12.0 (10.4)	Na_2SO_4 0.1 M 1.23 M Methanol Ar saturated	
300	80	Graphite	Ti/PbO_2	5	0.14 (0.12)	20.6 (17.9)	22.0 (19.0)	Na_2SO_4 0.1 M Ar saturated	
300	80	Graphite	Ti/PbO_2	5	2.79 (2.42)	15.3 (13.0)	19.7 (17.1)	Na_2SO_4 0.1 M 1.23 M Methanol Ar saturated	

follow–up study [15] employing NiO, CoO and MnO_2 likewise reported only limited enhancement at the optimum NiO loading (1.0 g L^{-1}), where hydrogen production increased from 37.8 to 40.7 μmol min^{-1} (US@EC/EC = 1.08), indicating that the introduction of solid catalysts does not necessarily guarantee a strong ultrasonic synergy and that the magnitude of enhancement is highly system–dependent.

Kerboua et al. [31] recently examined 490 kHz ultrasound in combination with alkaline electrolysis (1 M KOH, Ar saturation), explicitly separating the individual US, EC and US@EC contributions. Under their conditions, hydrogen generation rates of 5.69 μmol min^{-1} (US), 4.90 μmol min^{-1} (EC) and 8.95 μmol min^{-1} (US@EC) were obtained, corresponding to a synergy index below unity (US@EC/(EC + US) = 0.85), which suggests that ultrasound can in some cases interfere with, rather than enhance, electrochemical performance. Taken together, these literature reports demonstrate that sono–electrochemical synergy factors span a broad range from 0.8 to 1.5 depending on frequency, electrolyte, electrode configuration and catalyst usage, underscoring the need for systematic evaluation of operating parameters including saturation gas composition as explored in the present work to rationally design sonoelectrochemical systems that deliver reproducible and practically relevant enhancements in hydrogen production. The synergy factors of 1.06–1.14 obtained in this study (300 kHz US@EC system) fall toward the lower end of the reported range but remain highly reproducible and are achieved without the need for additional particulate catalysts or complex architectures.

4. Conclusion

The study demonstrates that coupling high–frequency ultrasound with electrolysis provides reproducible but moderate enhancements in hydrogen production, primarily through physical effects at the electrode/electrolyte interface rather than through direct sonochemical hydrogen generation. Methanol addition strongly boosts cavitation–-driven hydrogen formation and enables 300 kHz sonoelectrolysis to achieve synergy factors of 1.06–1.14 with maintained or even improved Faradaic efficiencies, while the choice of saturation gas (air, N_2, Ar) and modest changes in ionic strength only fine–tune the magnitude of this enhancement. At the same time, microscopy reveals that low–frequency operation at 28 kHz imposes substantially higher mechanical loads on Ti/PbO_2 and graphite electrodes than 300 kHz, confirming that bubble removal and mass–transfer benefits must be balanced against cavitation–induced electrode wear, especially under long–term potentiostatic operation.

Placed in the context of recent sono–electrolysis literature, the synergy factors achieved here fall toward the lower end of the reported 0.8–1.5 range but are obtained without particulate catalysts or complex cell architectures, and with a negligible absolute contribution from sonochemistry compared with electrochemical hydrogen production. These findings highlight that high–frequency ultrasound in the few–-hundred–kilohertz regime is particularly attractive for practical sonoelectrochemical hydrogen generation, as it consistently enhances current and hydrogen rates via bubble detachment and diffusion–layer renewal while limiting electrode damage and preserving charge efficiency. Future work focus on translating these insights into scalable reactor designs, optimizing acoustic coupling and cell geometry to maximize bubble–management benefits per unit acoustic power and rigorously assessing long–term stability and overall electrical–plus–acoustic energy efficiency under industrially relevant conditions.

CRediT authorship contribution statement

Jongbok Choi: Writing – review & editing, Writing – original draft, Project administration, Methodology, Investigation, Formal analysis, Data curation, Conceptualization. **Chaewoon Hwang:** Writing – original draft, Validation, Methodology, Investigation, Formal analysis, Data curation. **Younggyu Son:** Writing – review & editing, Writing – original draft, Supervision, Resources, Funding acquisition, Formal analysis, Conceptualization. **Muthupandian Ashokkumar:** Validation, Supervision, Resources, Investigation, Conceptualization.

Declaration of competing interest

The authors declare that they have no known competing financial interests or personal relationships that could have appeared to influence the work reported in this paper.

Acknowledgments

This work was supported by the National Research Foundation of Korea (NRF) grant funded by the Korean Government (MSIT) [RS-2024-00350023] and by Korea Environment Industry & Technology Institute (KEITI) through Soil Carbon Sequestration Project, funded by Korea Ministry of Climate, Energy and Environment (MCEE) [RS-2026-25501472].

Appendix A. Supplementary data

Supplementary data to this article can be found online at https://doi.org/10.1016/j.ultsonch.2026.107975.

References

[1] D. Tonelli, L. Rosa, P. Gabrielli, K. Caldeira, A. Parente, F. Contino, Global land and water limits to electrolytic hydrogen production using wind and solar resources, Nat. Commun. 14 (2023) 5532, https://doi.org/10.1038/s41467-023-41107-x.
[2] S. Karim, N. Tanwar, S. Das, R. Ranjit, A. Banerjee, A. Gulafshan, A. Gupta, A. D. Kumar, Shaping the future of green hydrogen production: Overcoming conventional challenges with molecular catalysts, immobilization, and scalable electrolyzers, ACS Catal. 15 (2025) 1073–1096, https://doi.org/10.1021/acscatal.4c05986.
[3] L. Wu, Q. Wang, S. Yuan, W. Li, X. Zou, M. Tang, K. Zhang, X. Yan, L. An, Bubble dynamics matters at high-rate water electrolysis, Nat. Commun. 17 (2026) 2305, https://doi.org/10.1038/s41467-026-69052-5.
[4] L. Li, P.C.M. Laan, X. Yan, X. Cao, M.J. Mekkering, K. Zhao, L. Ke, X. Jiang, X. Wu, L. Li, L. Xue, Z. Wang, G. Rothenberg, N. Yan, High-rate alkaline water electrolysis at industrially relevant conditions enabled by superaerophobic electrode assembly, Adv. Sci. 10 (2023) e2206180, https://doi.org/10.1002/advs.202206180.
[5] V. Agrež, Z. Heidary, M. Gavaises, R. Petkovšek, C.D. Ohl, Chladni figures reduce ohmic losses in alkaline electrolysis, Ultrason. Sonochem. (2026) 107833, https://doi.org/10.1016/j.ultsonch.2026.107833.
[6] H. Su, J. Sun, C. Wang, H. Wang, Study on the influence of ultrasound on the kinetic behaviour of hydrogen bubbles produced by proton exchange membrane electrolysis with water, Ultrason. Sonochem. 108 (2024) 106968, https://doi.org/10.1016/j.ultsonch.2024.106968.
[7] F. Foroughi, C. Immanuel Bernäcker, L. Röntzsch, B.G. Pollet, Understanding the effects of ultrasound (408 kHz) on the hydrogen evolution reaction (HER) and the oxygen evolution reaction (OER) on Raney-Ni in alkaline media, Ultrason. Sonochem. 84 (2022) 105979, https://doi.org/10.1016/j.ultsonch.2022.105979.
[8] M.H. Islam, B.G. Pollet, Perspective in the industrial applications of sonoelectrochemical hydrogen production, Curr. Opin. Chem. Eng. 48 (2025) 101122, https://doi.org/10.1016/j.coche.2025.101122.
[9] Y.H. Teoh, S.Y. Liew, H.G. How, H. Yaqoob, M.Y. Idroas, M.A. Jamil, S.U. Mahmud, T.D. Le, H.M. Ali, M.W. Shahzad, Investigating sono-electrolysis for hydrogen generation and energy optimization, Int. Commun. Heat Mass Transf. 164 (2025) 108980, https://doi.org/10.1016/j.icheatmasstransfer.2025.108980.
[10] B.G. Pollet, F. Foroughi, A.Y. Faid, D.R. Emberson, M.H. Islam, Does power ultrasound (26 kHz) affect the hydrogen evolution reaction (HER) on Pt polycrystalline electrode in a mild acidic electrolyte? Ultrason. Sonochem. 69 (2020) 105238 https://doi.org/10.1016/j.ultsonch.2020.105238.
[11] A. Pei, R. Xie, L. Zhu, F. Wu, Z. Huang, Y. Pang, Y.C. Chang, G. Chai, C.W. Pao, Q. Gao, C. Shang, G. Li, J. Ye, H. Zhu, Z. Yang, Z. Guo, Methanol-enhanced low-cell-voltage hydrogen generation at industrial-grade current density by triadic active sites of Pt_1–Pd_n–$(Ni,Co)(OH)_x$, J. Am. Chem. Soc. 147 (2025) 3185–3194, https://doi.org/10.1021/jacs.4c12665.
[12] N.K. Shrestha, A.I. Inamdar, H. Im, S. Cho, Boosting energy-efficient hydrogen evolution by electronically modulating Ni nodes in a framework for methanol oxidation in fresh and seawater, J. Mater. Chem. A 12 (2024) 29978–29988, https://doi.org/10.1039/D4TA05688D.
[13] Y. Xu, M. Liu, M. Wang, T. Ren, K. Ren, Z. Wang, X. Li, L. Wang, H. Wang, Methanol electroreforming coupled to green hydrogen production over bifunctional NiIr-based metal-organic framework nanosheet arrays, Appl Catal B 300 (2022) 120753, https://doi.org/10.1016/j.apcatb.2021.120753.
[14] C. Zeng, Y.H. Teoh, H. Geok How, M.Y. Idroas, T.D. Le, Ultrasound-enhanced water electrolysis for hydrogen production: Mechanisms, metrology and energy metrics, J. Electrochem. Sci. Eng. 16 (2026), https://doi.org/10.5599/jese.3045.
[15] Y.H. Teoh, W.Y. Han, H.G. How, H. Yaqoob, M.Y. Idroas, S.U. Mahmud, T.D. Le, M. Ahmad, M.W. Shahzad, Hydrogen production via electrolysis and ultrasound-assisted sonoelectrolysis: evaluating NiO, CoO, and MnO_2 catalyst performance and process efficiency, Energy Adv. (2026), https://doi.org/10.1039/D5YA00325C.
[16] J. Choi, S. Yoon, Y. Son, Effects of alcohols and dissolved gases on sonochemical generation of hydrogen in a 300 kHz sonoreactor, Ultrason. Sonochem. 101 (2023) 106660, https://doi.org/10.1016/j.ultsonch.2023.106660.
[17] S. Merouani, A. Dehane, O. Hamdaoui, Hydrogen production via water ultrasonication: a review, Ultrason. Sonochem. 120 (2025) 107515, https://doi.org/10.1016/j.ultsonch.2025.107515.
[18] Y. Zhou, Y. Ren, M. Cui, F. Guo, S. Sun, J. Ma, Z. Han, J. Khim, Sonoelectrochemical system mechanisms, design, and machine learning for predicting degradation kinetic constants of pharmaceutical pollutants, Chem. Eng. J. 478 (2023) 147266, https://doi.org/10.1016/j.cej.2023.147266.
[19] G. Li, G. Han, L. Wang, X. Cui, N.K. Moehring, P.R. Kidambi, D. Jiang, Y. Sun, Dual hydrogen production from electrocatalytic water reduction coupled with formaldehyde oxidation via a copper-silver electrocatalyst, Nat. Commun. 14 (2023) 525, https://doi.org/10.1038/s41467-023-36142-7.
[20] I. Roger, S. Rau, C. Streb, Sonochemical hydrogen production as a potential interference in light-driven hydrogen evolution catalysis, ACS Omega 5 (2020) 21250–21253, https://doi.org/10.1021/acsomega.0c03110.
[21] A. Dehane, S. Merouani, O. Hamdaoui, Methanol sono-pyrolysis for hydrogen recovery: effect of methanol concentration under an argon atmosphere, Chem. Eng. J. 433 (2022) 133272, https://doi.org/10.1016/j.cej.2021.133272.
[22] S.Z. Mikhail, W.R. Kimel, Densities and viscosities of methanol-water mixtures, J. Chem. Eng. Data 6 (1961) 533–537, https://doi.org/10.1021/je60011a015.
[23] P. Basařová, J. Pišlová, J. Mills, S. Orvalho, Influence of molecular structure of alcohol-water mixtures on bubble behaviour and bubble surface mobility, Chem. Eng. Sci. 192 (2018) 74–84, https://doi.org/10.1016/j.ces.2018.07.008.

[24] P.K. Mall, H.K. Paliwal, A. Medhavi, S. Ahmad, Effect of liquid density, ultrasonic velocity, and gas flow rate on the formation of air bubbles in aqueous methanol at temperature 293.15, 303.15, and 313.15 K, AIP Adv. 15 (2025), https://doi.org/10.1063/5.0251734.
[25] A. Dehane, S. Merouani, A. Chibani, O. Hamdaoui, M. Ashokkumar, Influence of processing conditions on hydrogen sonoproduction from methanol sono-conversion: a numerical investigation with a validated model, Chem. Eng. Process. 179 (2022) 109080, https://doi.org/10.1016/j.cep.2022.109080.
[26] N. Mahmood, Y. Yao, J.W. Zhang, L. Pan, X. Zhang, J.J. Zou, Electrocatalysts for hydrogen evolution in alkaline electrolytes: Mechanisms, challenges, and prospective solutions, Adv. Sci. 5 (2018) 1700464, https://doi.org/10.1002/advs.201700464.
[27] R. Pinto, M. Oliveira, A. Borges, An experimentally validated model of electrolyte effects in alkaline water electrolysis, Sci. Rep. 15 (2025) 41865, https://doi.org/10.1038/s41598-025-25842-3.
[28] C.R. Cloutier, D.P. Wilkinson, Electrolytic production of hydrogen from aqueous acidic methanol solutions, Int. J. Hydrog. Energy 35 (2010) 3967–3984, https://doi.org/10.1016/j.ijhydene.2010.02.005.
[29] N.H. Merabet, K. Kerboua, Membrane free alkaline sono-electrolysis for hydrogen production: an experimental approach, Int. J. Hydrog. Energy 49 (2024) 734–753, https://doi.org/10.1016/j.ijhydene.2023.09.061.
[30] S. Kwon, S. Bae, G. Son, Experimental study of ultrasound-assisted alkaline water electrolysis for hydrogen production, J. Mech. Sci. Technol. 39 (2025) 663–669, https://doi.org/10.1007/s12206-025-0113-9.
[31] K. Kerboua, M.H. Islam, N.H. Merabet, H.E. Hansen, F. Seland, O.S. Burheim, B. G. Pollet, Sono-electrolysis: a look into the distinguished effects of direct and indirect sonication at high frequency ultrasounds (490 kHz), Ultrason. Sonochem. 124 (2026) 107716, https://doi.org/10.1016/j.ultsonch.2025.107716.
[32] A. Saad, L. Bai, F.M.S. Christensen, S. Luo, A. Bentien, M. Ashokkumar, Z. Wei, Ultrasound-enhanced alkaline water splitting with fast bubble release and sustained Ni catalysts, Appl. Catal. B 370 (2025) 125152, https://doi.org/10.1016/j.apcatb.2025.125152.
[33] F. Araújo, R.C. Neto, A.S. Moita, Alkaline water electrolysis: ultrasonic field and hydrogen bubble formation, Int. J. Hydrog. Energy 78 (2024) 594–603, https://doi.org/10.1016/j.ijhydene.2024.06.263.
[34] Y.H. Teoh, P.H. Soon, H.G. How, H. Yaqoob, M.Y. Idroas, M.A. Jamil, S. U. Mahmud, T.D. Le, H.M. Ali, M.W. Shahzad, Optimization of catalyst for electrolysis and sono-electrolysis process for hydrogen production, Int. J. Hydrog. Energy 157 (2025) 150508, https://doi.org/10.1016/j.ijhydene.2025.150508.
[35] K.M. Cho, P.R. Deshmukh, W.G. Shin, Hydrodynamic behavior of bubbles at gas-evolving electrode in ultrasonic field during water electrolysis, Ultrason. Sonochem. 80 (2021) 105796, https://doi.org/10.1016/j.ultsonch.2021.105796.
[36] S. Merouani, A. Dehane, O. Hamdaoui, A review on the integration of ultrasonication in hybrid systems for enhanced hydrogen yield, Ultrason. Sonochem. 121 (2025) 107552, https://doi.org/10.1016/j.ultsonch.2025.107552.
[37] A.A. Kulkarni, J.B. Joshi, Bubble formation and bubble rise velocity in gas−liquid systems: a review, Ind. Eng. Chem. Res. 44 (2005) 5873–5931, https://doi.org/10.1021/ie049131p.
[38] Y. Son, J. Choi, Effects of gas saturation and sparging on sonochemical oxidation activity in open and closed systems, part II: NO_2^-/NO_3^- generation and a brief critical review, Ultrason. Sonochem. 92 (2023) 106250, https://doi.org/10.1016/j.ultsonch.2022.106250.
[39] J. Choi, Y. Son, Effect of dissolved gases on sonochemical oxidation in a 20 kHz probe system: continuous monitoring of dissolved oxygen concentration and sonochemical oxidation activity, Ultrason. Sonochem. 97 (2023) 106452, https://doi.org/10.1016/j.ultsonch.2023.106452.
[40] S. Lee, Y. Son, Effects of gas saturation and sparging on sonochemical oxidation activity under different liquid level and volume conditions in 300-kHz sonoreactors: zeroth- and first-order reaction comparison using KI dosimetry and BPA degradation, Ultrason. Sonochem. 98 (2023) 106521, https://doi.org/10.1016/j.ultsonch.2023.106521.
[41] K. Yasui, Influence of ultrasonic frequency on multibubble sonoluminescence, J. Acoust. Soc. Am. 112 (2002) 1405–1413, https://doi.org/10.1121/1.1502898.
[42] A. Brotchie, F. Grieser, M. Ashokkumar, Effect of power and frequency on bubble-size distributions in acoustic cavitation, Phys. Rev. Lett. 102 (2009) 084302, https://doi.org/10.1103/PhysRevLett.102.084302.